Bone 105 (2017) 67–74

Contents lists available at ScienceDirect

Bone

journal homepage: www.elsevier.com/locate/bone

Full Length Article

The fracture toughness of small animal cortical bone measured using arc-shaped tension specimens: Effects of bisphosphonate and deproteinization treatments

Michael D. Hunckler [a], Ethan D. Chu [a], Andrew P. Baumann [a], Tyler E. Curtis [a], Matthew J. Ravosa [a,b], Matthew R. Allen [c], Ryan K. Roeder [a,*]

[a] Department of Aerospace and Mechanical Engineering, University of Notre Dame, Notre Dame, IN 46556, USA
[b] Department of Biological Sciences, University of Notre Dame, Notre Dame, IN 46556, USA
[c] Department of Anatomy and Cell Biology, Indiana University School of Medicine, Indianapolis, IN 46202, USA

ARTICLE INFO

Article history:
Received 25 April 2017
Revised 17 August 2017
Accepted 17 August 2017
Available online 18 August 2017

Keywords:
Cortical bone
Fracture toughness
Bisphosphonates
Bone mineral density
Rabbit
Ulna

ABSTRACT

Small animal models, and especially transgenic models, have become widespread in the study of bone mechanobiology and metabolic bone disease, but test methods for measuring fracture toughness on multiple replicates or at multiple locations within a single small animal bone are lacking. Therefore, the objective of this study was to develop a method to measure cortical bone fracture toughness in multiple specimens and locations along the diaphysis of small animal bones. Arc-shaped tension specimens were prepared from the mid-diaphysis of rabbit ulnae and loaded to failure to measure the radial fracture toughness in multiple replicates per bone. The test specimen dimensions, crack length, and maximum load met requirements for measuring the plane strain fracture toughness. Experimental groups included a control group, bisphosphonate treatment group, and an *ex vivo* deproteinization treatment following bisphosphonate treatment (5 rabbits/group and 15 specimens/group). The fracture toughness of ulnar cortical bone from rabbits treated with zoledronic acid for six months exhibited no difference compared with the control group. Partially deproteinized specimens exhibited significantly lower fracture toughness compared with both the control and bisphosphonate treatment groups. The deproteinization treatment increased tissue mineral density (TMD) and resulted in a negative linear correlation between the measured fracture toughness and TMD. Fracture toughness measurements were repeatable with a coefficient of variation of 12–16% within experimental groups. Retrospective power analysis of the control and deproteinization treatment groups indicated a minimum detectable difference of 0.1 MPa·$m^{1/2}$. Therefore, the overall results of this study suggest that arc-shaped tension specimens offer an advantageous new method for measuring the fracture toughness in small animal bones.

1. Introduction

The mechanical characterization of small animal bones has received considerable interest with the widespread use of small animal models, and especially transgenic models, to investigate bone mechanobiology and metabolic bone disease [1–2]. A variety of test methods have been utilized to characterize the mechanical properties of whole small animal bones [3–6], including axial compression [7,8], torsion [6,9–11], and bending [4,6,9,10,12]. The cortex of small animal bones may also be machined into geometric specimens for destructive tests, such as beam bending and tensile testing [3,13,14], or non-destructive tests, such as (micro- or nano-) indentation [5,7,12,15] and ultrasonic wave propagation [3,16]. Cumulatively, these methods have greatly improved scientific understanding of bone tissue mechanics, bone quality, and metabolic bone disease, but provide limited insight into the fracture properties of whole small bones [2].

Strength-based measurements, such as the elastic modulus, yield stress, ultimate stress, and work to failure, are readily acquired during mechanical loading of un-notched geometric specimens [17]. However, small animal bones exhibit complex, non-uniform morphology, significant variability in morphology, and a heterogeneous distribution of tissue properties and defects (e.g., fatigue microcracks and porosity). These sources of heterogeneity inhibit accurate calculation of stress and strain using analytical solutions [18], and may thus require computational estimates using specimen-specific finite element models [19–21]. Moreover, the force required to initiate and propagate a crack to failure can be strongly influenced by heterogeneous tissue properties

* Corresponding author at: Department of Aerospace and Mechanical Engineering, Bioengineering Graduate Program, 148 Multidisciplinary Research Building, University of Notre Dame, Notre Dame, IN 46556, USA.
E-mail address: rroeder@nd.edu (R.K. Roeder).

http://dx.doi.org/10.1016/j.bone.2017.08.015
8756-3282/

and defects [22,23]. In contrast, a fracture mechanics approach introduces a critical size defect (sharp pre-crack) into the bone to direct crack initiation and propagation, while measuring the resistance to fracture, or fracture toughness [2]. Therefore, a fracture mechanics approach allows control over the location of fracture relative to tissue heterogeneity.

A novel method for measuring the fracture toughness of notched, whole rodent femora in three-point bending was previously developed using solutions for a circumferential through-wall crack in a cylindrical pipe [2,12]. However, this clever approach for measuring the fracture toughness of whole small animal bones only allows one measurement at one location per bone, which is a limitation shared with most destructive tests on small animal bones. The ability to measure fracture toughness on multiple replicates and/or at multiple locations within a single small animal bone post-mortem would be advantageous to increase study power via repeated measures, decrease the number of animals in a study, and enable site-specific measurements. For example, *in vivo* loading models in small animals (e.g., rabbit and rat ulnar loading) produce varying strain levels with maxima at specific locations along the length and around the perimeter of the diaphysis [19,20]. However, a test method does not yet exist for measuring fracture toughness on multiple replicates or at multiple locations within a single small animal bone.

Therefore, the objective of this study was to develop a method to measure cortical bone fracture toughness in multiple specimens and locations along the diaphysis of small animal bones. Arc-shaped tension specimens were prepared from the mid-diaphysis of rabbit ulnae and loaded in tension to failure to measure the plane strain fracture toughness in multiple replicates from a specific anatomic location of interest. Precision and sensitivity to detect differences were evaluated by testing specimens from multiple animals and treatments, including bisphosphonate-treated rabbits and deproteinized tissues.

2. Materials and methods

2.1. Animals and bisphosphonate treatment

Male New Zealand white rabbits were obtained at 4–6 months of age, such that all animals were skeletally mature [24]. Two cohorts included control ($N = 5$) and bisphosphonate-treated ($N = 10$) rabbits. Beginning at six months of age, bisphosphonate-treated rabbits were subjected to six intravenous bisphosphonate treatments at 30-day intervals (day 5, 35, 65, 95, 125, and 155). Rabbits in the control group were given saline injections on the same schedule. Bisphosphonate-treated rabbits received 0.1 mg/kg zoledronic acid (Zometa®, Novartis, East Hanover, NJ) diluted in 15 ml isotonic solution and administered intravenously over 15 min via an ear vein injection while under sedation [25]. Rabbits were housed in individual cages and allowed unrestricted movement and *ad libitum* access to food and water at all times. All rabbits were euthanized at 15–16 months of age by intravenous overdose of sodium pentobarbital (0.2 ml/kg, Somnasol, Butler-Schein, Dublin, OH), followed by bilateral pneumothorax. The mean (±standard deviation) body mass of the rabbits at sacrifice was 3.9 (0.3) kg for the control group and 3.6 (0.5) kg for the bisphosphonate-treated group. All experimental procedures were approved by the Institutional Animal Care and Use Committee at the University of Notre Dame prior to initiation of the study.

2.2. Specimen preparation

Left forelimbs were harvested from rabbits immediately following sacrifice and stored fresh-frozen at −20°C. Forelimbs were subsequently thawed at room temperature (~20°C) for 24 h. Ulnae were carefully removed from the forelimb, separated from the radius, and cleaned of all soft tissue by dissection while irrigated with phosphate buffered saline (PBS, Amresco, Inc., Solon, OH) to prevent tissue dehydration.

Arc-shaped tension specimens were prepared from the ulnar diaphysis at 50% of the total ulnar length (Fig. 1a). The total length of the ulna was measured from the ends of the olecranon (proximal) and styloid (distal) processes. Ulnae were sectioned perpendicular to the longitudinal axis of the bone using a low-speed diamond wire saw under continuous irrigation with deionized (DI) water. At least three transverse ulnar cross-sections, 1 mm in thickness, were sequentially sectioned beginning 2 mm distal to 50% of the total ulnar length and accounting for a wire kerf of 0.3 mm. A gap was cut into the cranial side of each ulnar cross-section to create arc-shaped tension specimens, which isolated the caudal side for tensile loading (Fig. 1c). As-prepared arc-shaped specimens were stored in PBS at 4°C for at least 12 h before notching.

Arc-shaped tension specimens (Fig. 2b) were notched on the endosteal surface of the caudal side of the ulnar cross-section such that the notch initiated a crack in the radial direction. The notch was cut using a low-speed diamond wire saw with a 0.3 mm diameter wire continuously irrigated with DI water. The notch was cut to a depth of ~0.12 mm using a custom fixture to ensure consistency. The resulting notch width at the endosteal surface was ~0.3 mm. A razor blade and 1 μm diamond slurry (MetaDi Diamond Paste, Buehler, Lake Bluff, IL) were used to create a sharp notch with a total depth, a, of ~0.15 mm and a root radius < 10 μm [2,26]. Proper depth and alignment of the sharp notch was controlled using a custom-specimen fixture and applying ~1 N force to the razor blade while cutting the sharp notch with a sawing motion [26]. Notched specimens were then rinsed with PBS (1X) to remove the diamond suspension.

Notched specimens were imaged at 100X magnification under an optical microscope (Eclipse ME600, Nikon Inc., Melville, NY) to verify the notch depth and alignment on both sides of the specimen (Fig. 2c). Notched specimens were also imaged by micro-CT (μCT-80, Scanco Medical AG, Brüttisellen, Switzerland) while submerged in PBS (1X) at 70 kVp, 114 μA, and 400 ms integration time, with a 20 μm voxel size for 250 projections per slice with image slices oriented perpendicular to the ulnar diaphysis using a 3D printed specimen holder. A representative image slice from the center of each specimen was segmented at a constant global threshold of 270, which corresponded to a tissue mineral density of ~840 mg hydroxyapatite per cubic centimeter (mg HA/cm^3) using a custom calibration phantom [27]. Segmented images were used to measure specimen-specific dimensions required for subsequent fracture toughness calculations described below.

2.3. Deproteinization treatment

Notched arc-shaped tension specimens from five randomly selected rabbits in the bisphosphonate-treated cohort were further subjected to deproteinization to validate the ability to measure small differences in fracture toughness. A pilot study first established appropriate conditions (immersion time) for achieving a small but measurable change in fracture toughness. As-prepared specimens ($n = 6$) were immersed in 5.25% sodium hypochlorite (NaOCl) at 20°C under constant rocking for 0.5, 1, 3, 6, 12, and 24 h. One group ($N = 5$ rabbits, $n = 15$ specimens) was then partially deproteinized by immersing as-prepared specimens in 5.25% NaOCl for 3 h at 20°C under constant rocking. Following immersion, specimens were rinsed under running water for approximately 30 min to prevent further effects of the deproteinization treatment [28,29].

All specimens were imaged by micro-CT before and after deproteinization treatments using the same methods described above. Control group specimens were also imaged by micro-CT before and after immersion in PBS for 3 h for comparison. A Gaussian filter (sigma = 0.8, support = 1.0) was applied to grayscale images to minimize high frequency noise. Bone tissue was segmented at a global threshold value of 270, which corresponded to a tissue mineral density of ~840 mg hydroxyapatite per cubic centimeter (mg HA/cm^3) using a custom calibration phantom [27]. Tissue mineral density (TMD) was measured within the segmented bone volume by converting the

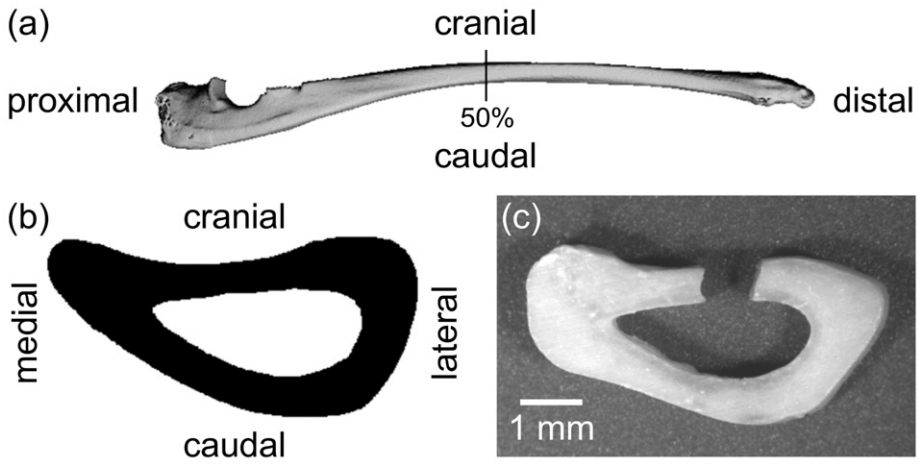

Fig. 1. (a) Segmented, 3-D micro-CT reconstruction of a rabbit ulna showing the location of transverse ulnar cross-sections prepared from the mid-diaphysis at 50% of the total ulnar length. (b) Segmented, 2-D micro-CT image slice showing a representative transverse ulnar cross-section from the mid-diaphysis and corresponding anatomic directions. (c) Photomicrograph showing a representative arc-shaped tension specimen with a gap cut into the cranial cortex to isolate the caudal cortex for tensile loading.

measured mean linear attenuation within the volume to mg HA/cm^3 using the same calibration phantom [27].

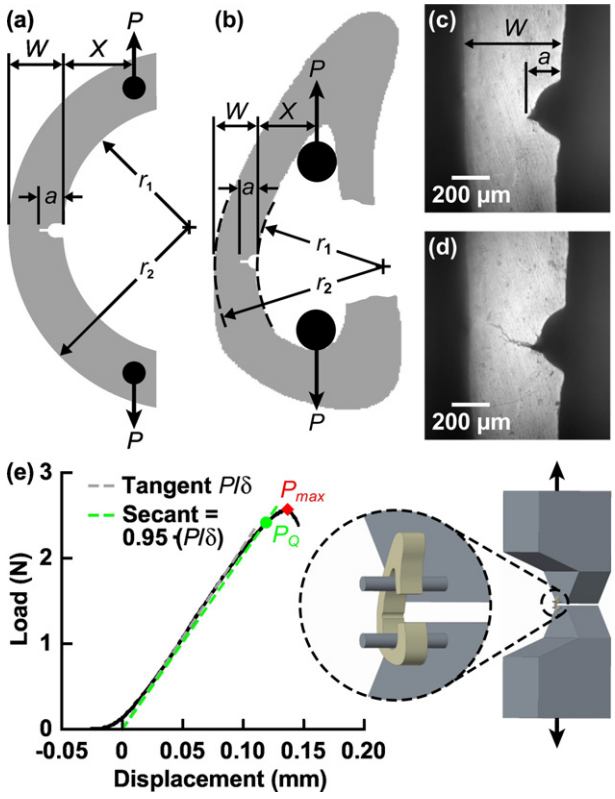

Fig. 2. Schematic diagram showing (a) the ASTM E399 [30] standard geometry for arc-shaped tension specimens compared with (b) a representative ulnar cross-section as imaged by micro-CT, and the applied load, *P*. Segmented micro-CT images were used to measure the internal radius, r_1, external radius, r_2, and distance between the notch mouth and load line, *X*. Optical micrographs at 100X magnification were used to (c) measure the notch depth, *a*, and cortical width, *W*, for each specimen before testing, and (d) verify that a crack initiated in the radial direction at the notch tip after testing. (e) Load-displacement data collected for a representative ulnar arc-shaped tension specimen showing the identification of the conditional load, P_Q, maximum load, P_{max}, tangent stiffness, P/δ, and secant stiffness, $0.95 \cdot P/\delta$, used to calculate the fracture toughness, K_{Ic}, following ASTM E399 guidelines [30]; schematic diagram showing the custom fixture for loading ulnar arc-shaped tension specimens via two hardened steel pins, 0.63 mm in diameter.

2.4. Fracture toughness testing

Experimental methods and calculations for measuring fracture toughness followed guidelines for arc-shaped specimens outlined in ASTM E399 unless otherwise noted below [30]. Notched arc-shaped tension specimens (Fig. 2) were loaded (ElectroForce 3220, Bose Corp., Eden Prarie, MN) to failure at a displacement rate of 0.02 mm/s, such that the time to reach the maximum load was at least 0.3 min, while hydrated in PBS (1X) at ambient temperature. Specimens were loaded using a custom fixture comprising two hardened steel pins, 0.63 mm in diameter, press-fit into two aluminum blocks (Fig. 2e). Axial load-displacement data was collected for each specimen using a 50 lbf load cell (Interface, Scottsdale, AZ) and linear variable displacement transducer, respectively, at a sampling rate of 250 Hz. Fractured specimens were imaged by optical microscopy (Nikon ME600) at 100X magnification to verify that fracture initiated at the sharp notch (Fig. 2d).

The conditional fracture toughness, K_Q, measured from arc-shaped tension specimens (Fig. 2) was calculated as [30],

$$K_Q = \frac{P_Q}{B\sqrt{W}}\left(3\frac{X}{W} + 1.9 + 1.1\frac{a}{W}\right)\left[1 + 0.25\left(1-\frac{a}{W}\right)^2\left(1-\frac{r_1}{r_2}\right)\right] \cdot f\left(\frac{a}{W}\right) \quad (1)$$

where P_Q is the conditional load, *B* is the specimen breadth, *W* is the cortical width or thickness, *X* is loading line offset, *a* is the notch depth, r_1 is the inner radius, r_2 is the outer radius, and

$$f\left(\frac{a}{W}\right) = \frac{\sqrt{\frac{a}{W}}}{\left(1-\frac{a}{W}\right)^{3/2}}\left[3.74 - 6.30\frac{a}{W} + 6.32\left(\frac{a}{W}\right)^2 - 2.43\left(\frac{a}{W}\right)^3\right]. \quad (2)$$

The calculated conditional fracture toughness, K_Q, is equal to the linear elastic plane strain fracture toughness, K_{Ic}, when two conditions are fulfilled: (1) $P_{max}/P_Q < 1.10$ and (2) *B*, *a*, and $(W\text{-}a) > 2.5(K_{Ic}/\sigma_{ys})^2$, where σ_{ys} is the material yield strength.

The conditional load, P_Q, was determined by the intersection of the load-displacement data and a secant line with slope equal to $0.95 \cdot (P/\delta)$, where P/δ is the tangent stiffness measured as the maximum slope of the load-displacement data using linear least squares regression (MATLAB 9.0, The MathWorks, Inc., Natick, MA) (Fig. 2e). P_{max} was determined as the maximum load during the test. If the displacement at P_Q exceeded the displacement at P_{max}, which occurred for two specimens, then $P_Q = P_{max}$ per ASTM E399 guidelines [30]. The mean (±

standard deviation) P_{max}/P_Q ratio for all specimens was 1.06 (0.06), which was significantly lower than the maximum value of 1.10 allowed by ASTM E399 [30] for plane strain conditions ($p < 0.0001$, Wilcoxon signed-rank test vs. 1.10).

Specimen dimensions used in the fracture toughness calculations were measured from segmented micro-CT images of each notched arc-shaped tension specimen using a custom automated script (MATLAB 9.0) which positioned the loading pins within the medullary space by maximizing the distance between the pins the same as occurred during loading (Fig. 2b). The load line offset, X, was the perpendicular distance from the load line to the endosteal surface. The cortical thickness of the ulna, W, was the distance between the endosteal and periosteal surfaces, and was taken as the average of measurements on either side of the notch and on both surfaces (Fig. 2c). The arc radius of the endosteal surface, r_1, was approximated by a circular fit minimizing the sum of squared radial deviations over a contour spanning ± 1 mm from the notch (Fig. 2b). The arc radius of the periosteal surface, r_2, was approximated by extending r_1 to the periosteal surface while maintaining concentric circles for r_1 and r_2. The thickness of the specimen, B, was taken as the average of measurementson either side of the notch using digital calipers. The notch depth, a, was the perpendicular distance from the endosteal surface to the notch tip, and was taken as the average of measurements on both sides of the specimen using an optical microscope (Nikon ME600) at 100X magnification (Fig. 2c). After fracture toughness tests, the angle between the direction of crack propagation and the load line normal, β, as well as the normal to endosteal tangent line, was measured for each specimen.

2.5. Statistical methods

The normality of all experimental measurements was verified using the Shapiro-Wilk test (JMP 12.1.0, SAS Institute, Inc., Cary, NC). Differences in K_{Ic} and the change in TMD between experimental groups ($n = 15$ specimens/group), were examined using mixed model analysis of variance (ANOVA) accounting for repeated measures (3/rabbit) from each animal ($N = 5$ rabbits) and the nested, random effect of the animal. Post hoc comparisons were performed using Student's t-tests with a Bonferroni correction for multiple comparisons. The relationship between K_{Ic} and immersion time, and K_{Ic} and TMD, for the deproteinized specimens was fit using linear least squares regression. The TMD of specimens before and after immersion in PBS (control) or NaOCl (deproteinization) ($n = 15$ specimens/group) was compared using paired t-tests. A measured change in TMD greater than zero was also confirmed using one-sample Student's t-tests with a hypothesized mean of zero. The level of significance for all tests was set at $p < 0.05$.

3. Results

3.1. Fracture toughness measurements

The mean (±standard deviation) radial fracture toughness was 1.07 (0.14) MPa·m$^{1/2}$ for the control group, 1.11 (0.13) MPa·m$^{1/2}$ for the bisphosphonate treatment group, and 0.83 (0.13) MPa·m$^{1/2}$ for the deproteinization treatment group (Fig. 3). Deproteinized specimens exhibited significantly lower fracture toughness compared with both the control and bisphosphonate treatment groups ($p < 0.0005$, t-test) (Fig. 3). The difference between the control and bisphosphonate treatment groups was not statistically significant ($p = 0.38$). Importantly, fracture toughness measurements exhibited a coefficient of variation of 13% for the control group, 12% for the bisphosphonate treatment group, and 16% for the deproteinization treatment group. The geometric dimensions of ulnar arc-shaped tension specimens exhibited similar consistency, with coefficients of variation ranging from 5.8 to 17.7% (Table 1).

Fracture analysis revealed that all ulnar arc-shaped ulnar tension specimens exhibited crack initiation at the notch tip and propagation along a similar path perpendicular to the endosteal surface, regardless of the experimental group (Fig. 2d). The pooled mean (±standard deviation) angle between the direction of crack propagation and the normal to endosteal tangent line was 0.6 (6.8)°. The mean (±standard deviation) angle between the direction of crack propagation and the load line normal (β) was 9.0 (7.4)° for the control group, 11.0 (6.6)° for the bisphosphonate treatment group, and 5.7 (4.9)° for deproteinization treatment group, but differences between experimental groups were not statistically significant ($p > 0.11$, ANOVA). The crack path also exhibited no qualitative differences between experimental groups.

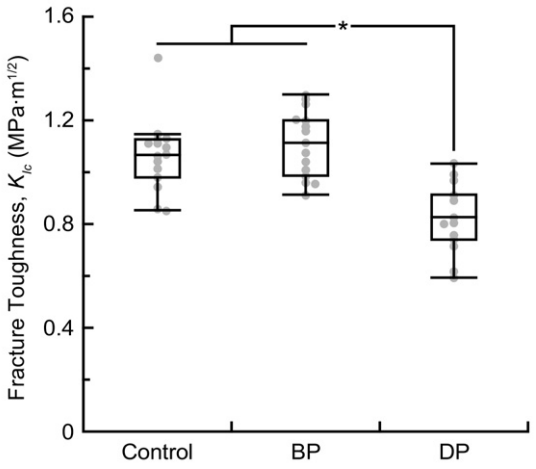

Fig. 3. The measured fracture toughness, K_{Ic}, of arc-shaped tension specimens prepared from control, bisphosphonate (BP)-treated, and deproteinized (DP) ulnar cortical bone tissue. The box and whiskers show the 5th, 25th, 50th (median), 75th, and 95th percentiles. Deproteinized specimens exhibited a significantly lower fracture toughness compared with both the control and bisphosphonate treatment groups (*$p < 0.0005$, t-test). The difference between the control and bisphosphonate treatment groups was not statistically significant ($p = 0.38$).

3.2. Deproteinization treatment and tissue mineral density

A pilot study was conducted to establish suitable deproteinization conditions by immersing specimens in NaOCl for varying amounts of time (Fig. 4). The measured fracture toughness exhibited a negative linear relationship with immersion time ($p < 0.05$, $R^2 = 0.81$). The fracture toughness was decreased by ~10% after 3 h, which was chosen as the immersion time for the deproteinization treatment group reported above.

The tissue mineral density (TMD) of the ulnar arc-shaped tension specimens was measured before and after immersion in PBS and NaOCl for the control and deproteinization treatment groups, respectively (Fig. 5). TMD was significantly increased for the deproteinized specimens ($p < 0.005$, paired t-test), but not for the control specimens ($p = 0.46$, paired t-test) (Fig. 5a and b). The mean (±standard deviation) change in TMD was 3.2 (15.8) and 15.1 (15.5) mg HA/cm^3 for the control and deproteinization groups, respectively (Fig. 5c). The change in TMD was statistically significant for deproteinization ($p < 0.005$, t-test vs. 0), but not the control treatment ($p = 0.46$), and the hypothesized difference between the treatments was statistically significant ($p < 0.05$, t-test). The measured fracture toughness of

Table 1
Ulnar arc-shaped tension specimen dimensions showing the mean (± standard deviation) and coefficient of variation.

Variable	Dimension	Coefficient of Variation (%)
a	0.15 (0.02) mm	12.2
W	0.63 (0.08) mm	12.3
X	0.84 (0.15) mm	17.7
r_1/r_2	0.76 (0.06)	7.7
B	0.99 (0.06) mm	5.8

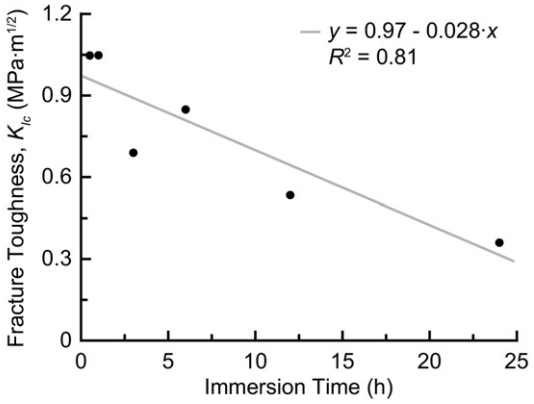

Fig. 4. The measured fracture toughness, K_{Ic}, of ulnar arc-shaped tension specimens exhibited a negative linear relationship with the immersion time for deproteinization treatment ($p < 0.05$, $R^2 = 0.81$).

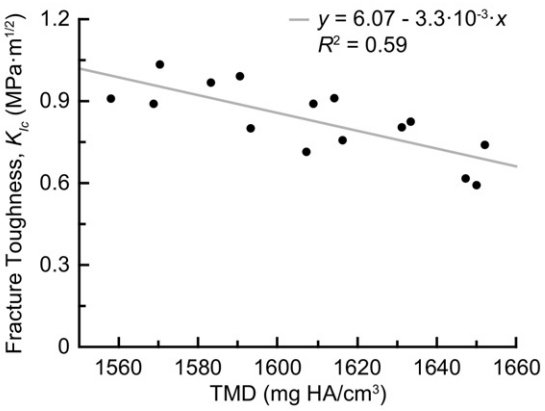

Fig. 6. The measured fracture toughness, K_{Ic}, exhibited a negative linear correlation with the measured TMD of deproteinized, ulnar arc-shaped tension specimens ($p < 0.001$, $R^2 = 0.59$).

deproteinized specimens exhibited a negative linear correlation with TMD ($p < 0.001$, $R^2 = 0.59$) (Fig. 6).

4. Discussion

4.1. Validity of linear-elastic plane strain fracture toughness

A valid measurement of the plane strain fracture toughness, K_{Ic}, requires conditions of plane strain and small-scale yielding at the crack tip [30]. Limited plasticity at the crack tip was ensured with the requirement that $P_{max}/P_Q < 1.10$. Previous methods for measuring K_{Ic} in small animal bones have not been able to meet this criteria [2]. However, in this study, we achieved a mean (±standard deviation) of P_{max}/P_Q of 1.06 (0.06), with only 6 of 45 specimens marginally exceeding $P_{max}/P_Q = 1.10$.

Small-scale yielding at the crack tip requires that the plastic zone is small compared to the in-plane dimensions of the crack size, a, specimen breadth, B, and uncracked ligament length, W-a. This is expressed as a single criterion,

$$B, a, (W-a) > 2.5\left(\frac{K_{Ic}}{\sigma_{ys}}\right)^2 \quad (3)$$

where σ_{ys} is the material yield strength. The plastic zone for specimens in this study was estimated to be ~0.33 mm, using the measured K_{Ic} (~1.0 MPa·m$^{1/2}$) and σ_{ys} (~87 MPa, Appendix 1) for arc-shaped tension specimens in this study. Therefore, mean (±standard deviation) specimen breadth, $B = 0.99$ (0.06) mm, and uncracked ligament length, W-$a = 0.63$ (0.08) mm, were significantly greater than the size of the plastic zone, satisfying the plane strain condition. The mean (±standard deviation) crack size, $a = 0.15$ (0.02) mm, was less than the plastic zone size. However, the ASTM small-scale yielding criteria has been noted to be conservative because it was designed for metals and not more brittle materials such as bone [2].

Therefore, fracture toughness measurements in this study are considered to be close estimates of the true linear-elastic plane strain fracture toughness, K_{Ic}. Nonetheless, the measured magnitude of K_{Ic} should only be compared to measurements obtained using similar testing geometries and specimen dimensions. Fracture toughness measurements are inherently dependent on the specimen geometry, specimen size, animal species, crack orientation, and test method (e.g., compact tension, arc-shaped tension, single-edged notched tension or beam, etc.) [31]. Importantly, the coefficient of variation in the fracture toughness measured by arc-shaped tension specimens in this study was 12–16%, which compares favorably to a coefficient of variation ranging from 9–22% for fracture toughness measurements on small bone specimens using other methods [2].

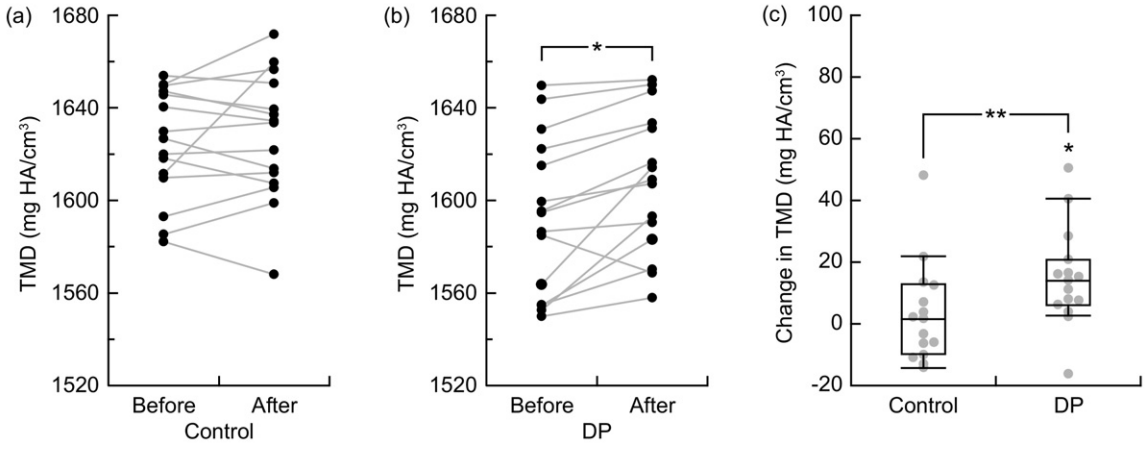

Fig. 5. The tissue mineral density (TMD) of ulnar arc-shaped tension specimens before and after (a) immersion in PBS (1X) for 3 h (control) and (b) deproteinization by immersion in NaOCl for 3 h. The measured TMD was increased after the deproteinization treatment (*$p < 0.005$, paired t-test) but not the control treatment ($p = 0.46$). (c) The measured change in the TMD of ulnar arc-shaped tension specimens after the control or deproteinization treatment. The box and whiskers show the 5th, 25th, 50th (median), 75th, and 95th percentiles. The change in TMD was statistically significant for deproteinization ($p < 0.005$, t-test vs. 0), but not the control treatment ($p = 0.46$), and the hypothesized difference between the treatments was statistically significant (**$p < 0.05$, t-test).

4.2. Radial fracture toughness

The fracture toughness of bone is well-known to be anisotropic due to differences in toughening mechanisms for different crack orientations [31–34]. For example, the fracture toughness of human cortical bone in the transverse direction was 51% higher than the longitudinal direction and 140% higher than the radial direction [34]. In human cortical bone, cracks propagating transverse to the osteonal direction exhibit the highest fracture toughness due to extrinsic toughening from macroscopic crack deflection [31]. Cracks propagating in the longitudinal direction exhibit lower fracture toughness due to the crack readily splitting osteons with less deflection and crack bridging becoming the dominant toughening mechanism [32]. Cracks propagating in the radial direction exhibit the lowest fracture toughness due to smaller bridging zones compared with the longitudinal direction [33]. Thus, cracks propagating in the radial-longitudinal plane follow inter-osteonal paths along cement lines with relatively little deflection compared with transverse cracks [31–34].

The arc-shaped tension specimens in this study measured fracture toughness for crack propagation in the radial direction of the cortical bone tissue (Fig. 2) rather than the longitudinal or transverse directions. Therefore, the fracture toughness measured in this study for the control group (~1.1 $MPa \cdot m^{1/2}$) was lower than previous measurements in the longitudinal direction of non-pathological human humeral cortical bone (~1–2 $MPa \cdot m^{1/2}$) using single-edge notched beams [31] and rabbit tibial cortical bone (~1.4 $MPa \cdot m^{1/2}$) using compact tension specimens [35], as would be expected, notwithstanding the aforementioned caution in comparing measurements obtained using different test specimen geometry and dimensions.

4.3. Effects of bisphosphonate treatment

In this study, skeletally mature male rabbits were treated with six 0.1 mg/kg doses of zoledronic acid over 6 months and this bisphosphonate treatment had no effect on the ulnar cortical bone fracture toughness (K_{Ic}) measured by arc-shaped tension specimens (Fig. 3). Bisphosphonate treatments are known to maintain or improve whole bone mechanical properties through the preservation of bone mass, but the effects of bisphosphonate treatments on tissue material properties have been mixed [12,13]. A number of preclinical studies have reported that tissue material properties of long bones were not altered by bisphosphonate treatment. Rabbits treated with zoledronic acid over 4 weeks [36], pamidronate over 7 weeks [11], and alendronate over 13 weeks [37] exhibited no effect on tissue material properties estimated from flexural and torsional loading of whole tibiae and femora. Canines subjected to daily alendronate treatment for up to 3 years exhibited no statistically significant effects on the tensile or flexural mechanical properties of femoral [38,39] and humeral [40] cortical bone compared to controls. Importantly, the fracture toughness (K_{Ic}) and *R*-curve behavior of femoral or humeral cortical bone in canines subjected to daily alendronate treatment for up to 3 years [38,40], and of femoral cortical bone in rats treated with either risedronate or ibandronate for 4 months [12], was not statistically different from controls. In contrast to the aforementioned studies, canines treated with alendronate for up to 3 years were reported to exhibit compromised cortical bone tissue material properties, namely the post-yield toughness (modulus of toughness), measured by differences in the area under the stress-strain curve for flexural loading of whole ribs [41–44]. Moreover, the fatigue resistance of cortical bone specimens machined from canine ribs was compromised after treatment with alendronate over 3 years [13]. One potential explanation for the discrepancy among these studies is that higher rates of bone turnover in the rib (~20%/year) compared with long bones (typically 1–2%/year) may accentuate the effects bisphosphonate treatment on tissue material properties.

4.4. Effects of deproteinization treatment

In order to validate sensitivity to detect differences in fracture toughness with arc-shaped tension specimens, a group of bisphosphonate-treated specimens was further subjected to 3 h immersion in NaOCl to partially deproteinize tissue before fracture toughness testing. The effect of this deproteinization treatment was further validated by demonstrating a significant increase in TMD compared with the control group (Fig. 5). Deproteinization of bone via immersion in NaOCl is known to facilitate progressive removal of the organic matrix and extensive microcrack accumulation, resulting in reduced mechanical strength [28,29]. The organic matrix of bone is a continuous phase that separates and binds the apatite bone mineral crystals together. Therefore, the measured decrease in fracture toughness after deproteinization treatment (Fig. 3) was most likely due to the partial and progressive removal of the organic matrix near specimen surfaces resulting in collapse or percolation of the mineral phase, which would be expected to increase TMD and decrease fracture toughness (Figs. 5 and 6).

Retrospective power analysis of fracture toughness measurements for the control and deproteinization treatment groups indicated a minimum detectable difference of 0.1 $MPa \cdot m^{1/2}$ for a variance of 0.018. The coefficient of variation for the control and deproteinization treatment groups was 12 and 16%, respectively. Therefore, the fracture toughness of small animal bones measured using arc-shaped tension specimens exhibited sufficient precision and sensitivity to detect small differences.

4.5. Advantages and limitations

Arc-shaped tension specimens offer a new, advantageous method for measuring the fracture toughness in small animal bones. The specimen geometry allows many specimens to be prepared from a small amount of tissue in a single small animal bone. For example, a two-centimeter segment of the mid-diaphysis of the rabbit ulna can yield approximately 15 similarly shaped ulnar cross-sections that can be processed into arc-shaped tension specimens. Therefore, a repeated measures design facilitates an increased sample size per animal and thus increased statistical power by decreasing random variability in the fracture toughness measured for a single animal. Moreover, multiple transverse sections may be simultaneously cut from a single small animal bone to facilitate both histology and fracture toughness testing on adjacent tissue sections. Alternating specimens could be paired for analysis. However, the potential for significant deviations in the ulnar cross-sectional geometry must be considered when sampling from multiple anatomic locations. Therefore, the effect of sampling from multiple anatomic locations must either be shown to be not significant, as was the case in this study ($p > 0.30$, ANOVA), or accounted for by multifactorial statistical analyses.

Arc-shaped tension specimens also enable the measurement of fracture toughness at specific anatomic locations within a single small animal bone. For example, *in vivo* ulnar loading can produce periosteal bone formation [19] and microdamage [45] at locations of maximum tissue strain on the caudal surface near the mid-diaphysis of ulnae. The notch was created at this location of maximum strain in the ulnar cross-section. Therefore, arc-shaped tension specimens could potentially investigate the effects of *in vivo* loading on post-mortem local tissue mechanical properties at specified anatomic locations. The radial fracture toughness measured with arc-shaped tension specimens is expected to be particularly sensitive to the presence of longitudinal microcracks that form at weak microstructural interfaces during compressive loading [46]. Importantly, the methods demonstrated in this study for rabbit ulnae can be readily adapted for other small animal bones, such as rat or rabbit tibiae, femora, humeri, radii, etc. For example, transverse sections from rat femora are of similar size compared with the rabbit ulnar cross-sections in this study. On the other hand,

testing of mouse bones is not likely feasible with this method, at least not with a conventional mechanical testing load frame.

Deviations between the ASTM standard geometry and the actual geometry of arc-shaped tissue specimens (Fig. 2), as well as variability in the cortical thickness, likely resulted in asymmetric loading at the notch of arc-shaped tension specimens. However, the pooled mean (±standard deviation) crack angle, β, of 8.6 (6.6)° suggests that the contribution of mode II loading was only ~15% of that for pure mode I loading, due to the relative mode II contribution scaling with $\sin(\beta)\cos(\beta)$ [47]. Moreover, the pooled mean (±standard deviation) angle between the direction of crack propagation and the normal to endosteal tangent line was also measured as 0.6 (6.8)°. This suggests that the direction of crack propagation was primarily governed by the shortest distance between the notch and the periosteal surface and the contribution of mode II loading was even less than that suggested by the crack angle, β. Thus, the effect of differences and variability in the geometry of arc-shaped tension specimens compared to the ASTM standard geometry on stress intensity solutions should be examined more rigorously using finite element modeling.

The methods of this study were not without other limitations, primarily due to the small specimen size. The measurement of *R*-curve behavior is possible but likely challenging due to the small specimen size (*W*-*a*) and limited *R*-curve behavior expected for radial crack propagation [2,31]. Thus, arc-shaped tension specimens were used in this study to measure the initiation fracture toughness and not the propagation toughness or *R*-curve. The small specimens also required customized fixtures to aid specimen preparation (e.g., notching) and tensile loading (Fig. 2).

Disclosures

R.K. Roeder has received research grants from Merck Sharp & Dohme Corp. M.R. Allen has received research grants from Amgen Inc., Eli Lilly and Company, and Merck Sharp & Dohme Corp. All other authors have no potential conflicts of interest.

Acknowledgments

This research was supported by a Collaboration in Translational Research (CTR) pilot grant from the Indiana Clinical and Translational Sciences Institute (CTSI) (NIH RR025761) and an Advancing Basic Cancer (ABC) Research grant from the Walther Cancer Foundation. The authors thank the staff of the Freimann Life Science Center at Notre Dame for their assistance in caring for the rabbits.

Appendix 1. Estimation of tissue yield strength from arc-shaped tensile specimens

The tissue yield strength, σ_{ys}, in Eq. (3) was measured using unnotched arc-shaped tensile specimens that were otherwise prepared and loaded using the same methods described above. The absence of a notch and variations in the cortical thickness led to fracture at various locations. Therefore, measurements were collected only for specimens that fractured at the same location where a notch would have been placed ($n = 5$ specimens/group). The yield strength was calculated as [48],

$$\sigma_{ys} = \frac{F_y}{WB} + \frac{M_y W}{2I} \tag{4}$$

where F_y is the load at yielding, W is the cortical thickness at the fracture site, B is the specimen thickness, M_y is the moment at yielding ($= F_y(X + W/2)$), and I is the cross-sectional moment of inertia ($BW^3/12$). The load at yielding was measured using a 0.01 mm offset displacement to the tangent stiffness, P/δ, to approximate a 0.2% offset strain. The pooled mean (±standard deviation) fracture strength was measured to be 87 (10) MPa. The effect of the experimental group was not statistically significant ($p > 0.28$, ANOVA).

References

[1] D. Vashishth, Small animal bone biomechanics, Bone 43 (2008) 794–797, http://dx.doi.org/10.1016/j.bone.2008.06.013.
[2] R.O. Ritchie, K.J. Koester, S. Ionova, W. Yao, N.E. Lane, J.W. Ager, Measurement of the toughness of bone: a tutorial with special reference to small animal studies, Bone 43 (2008) 798–812, http://dx.doi.org/10.1016/j.bone.2008.04.027.
[3] C.H. Turner, D.B. Burr, Basic biomechanical measurements of bone: a tutorial, Bone 14 (1993) 595–608, http://dx.doi.org/10.1016/8756-3282(93)90081-K.
[4] C.H. Turner, R.K. Roeder, A. Wieczorek, T. Foroud, G. Liu, M. Peacock, Variability in skeletal mass, structure, and biomechanical properties among inbred strains of rats, J. Bone Miner. Res. 16 (2001) 1532–1539, http://dx.doi.org/10.1359/jbmr.2001.16.8.1532.
[5] E. Donnelly, Methods for assessing bone quality: a review, Clin. Orthop. Relat. Res. 469 (2011) 2128–2138, http://dx.doi.org/10.1371/journal.pone.0119603.
[6] M. Steiner, D. Volkheimer, N. Meyers, T. Wehner, H.-J. Wilke, L. Claes, A. Ignatius, Comparison between different methods for biomechanical assessment of *ex vivo* fracture callus stiffness in small animal healing studies, PLoS ONE 10 (2016), e0119603. http://dx.doi.org/10.1371/journal.pone.0119603.
[7] E. Cory, A. Nazarian, V. Entezari, V. Vartanians, R. Müller, B.D. Snyder, Compressive axial mechanical properties of rat bone as functions of bone volume fraction, apparent density and micro-CT based mineral density, J. Biomech. 43 (2010) 953–960, http://dx.doi.org/10.1016/j.jbiomech.2009.10.047.
[8] N.A. Danova, S.A. Colopy, C.L. Radtke, V.L. Kalscheur, M.D. Markel, R. Vanderby Jr., R.P. McCabe, A.J. Escarcega, P. Muir, Degradation of bone structural properties by accumulation and coalescence of microcracks, Bone 33 (2003) 197–205, http://dx.doi.org/10.1016/S8756-3282(03)00155-8.
[9] L.B. Engesæter, A. Ekeland, N. Langeland, Methods for testing the mechanical properties of the rat femur, Acta Orthop. Scand. 49 (1978) 512–518, http://dx.doi.org/10.3109/17453677808993231.
[10] A. Ekeland, L.B. Engesæter, N. Langeland, Mechanical properties of fractured and intact rat femora evaluated by bending, torsional and tensile tests, Acta Orthop. Scand. 52 (1981) 605–613, http://dx.doi.org/10.3109/17453678108992155.
[11] C.M. Bellingham, J.M. Lee, E.L. Moran, E.R. Bogoch, Bisphosphonate (pamidronate/APD) prevents arthritis-induced loss of fracture toughness in the rabbit femoral diaphysis, J. Orthop. Res. 13 (1995) 876–880, http://dx.doi.org/10.1002/jor.1100130611.
[12] M. Shahnazari, W. Yao, W.W. Dai, B. Wang, S.S. Ionova-Martin, R.O. Ritchie, D. Heeren, A.J. Burghardt, D.P. Nicolella, M.G. Kimiecik, N.E. Lane, Higher doses of bisphosphonates further improve bone mass, architecture, and strength, but not the tissue material properties in aged rats, Bone 46 (2010) 1267–1274, http://dx.doi.org/10.1016/j.bone.2009.11.019.
[13] D. Bajaj, J.R. Geissler, M.R. Allen, D.B. Burr, J.C. Fritton, The resistance of cortical bone tissue to failure under cyclic loading is reduced with alendronate, Bone 64 (2014) 57–64, http://dx.doi.org/10.1016/j.bone.2014.03.045.
[14] J.G. Ramasamy, O. Akkus, Local variations in the micromechanical properties of mouse femur: the involvement of collagen fiber orientation and mineralization, J. Biomech. 40 (2007) 910–918, http://dx.doi.org/10.1016/j.jbiomech.2006.03.002.
[15] P.K. Zysset, Indentation of bone tissue: a short review, Osteoporos. Int. 20 (2009) 1049–1055, http://dx.doi.org/10.1007/s00198-009-0854-9.
[16] S.S. Kohles, J.R. Bowers, A.C. Vailas, R. Vanderby Jr., Ultrasonic wave velocity measurement in small polymeric and cortical bone specimens, J. Biomech. Eng. 119 (1997) 232–236, http://dx.doi.org/10.1115/1.2796085.
[17] R.K. Roeder, Mechanical characterization of biomaterials, in: A. Bandyopadhyay, S. Bose (Eds.), Characterization of Biomaterials, Elsevier, Amsterdam 2013, pp. 49–104, http://dx.doi.org/10.1016/B978-0-12-415800-9.00003-6.
[18] G.H. van Lenthe, R. Voide, S.K. Boyd, R. Müller, Tissue modulus calculated from beam theory is biased by bone size and geometry: implications for the use of three-point bending tests to determine bone tissue modulus, J. Biomech. 43 (2008) 717–723, http://dx.doi.org/10.1016/j.bone.2008.06.008.
[19] A.P. Baumann, M.W. Aref, T.L. Turnbull, A.G. Robling, G.L. Niebur, M.R. Allen, R.K. Roeder, Development of an *in vivo* rabbit ulnar loading model, Bone 75 (2015) 55–61, http://dx.doi.org/10.1016/j.bone.2015.01.022.
[20] S.P. Kotha, Y.F. Hsieh, R.M. Strigel, R. Müller, M.J. Silva, Experimental and finite element analysis of the rat ulnar loading model—correlations between strain and bone formation following fatigue loading, J. Biomech. 37 (2004) 541–548, http://dx.doi.org/10.1016/j.jbiomech.2003.08.009.
[21] J.A. Gargac, T.L. Turnbull, R.K. Roeder, G.L. Niebur, A probabilistic damage model based on direct 3-D correlation of strain to damage formation following fatigue loading of rat femora, J. Mech. Behav. Biomed. Mater. 30 (2014) 234–243, http://dx.doi.org/10.1016/j.jmbbm.2013.11.009.
[22] K.S. Chan, D.P. Nicolella, Micromechanical modeling of *R*-curve behaviors in human cortical bone, J. Mech. Behav. Biomed. Mater. 16 (2012) 136–152, http://dx.doi.org/10.1016/j.jmbbm.2012.09.009.
[23] T.L. Turnbull, A.P. Baumann, R.K. Roeder, Fatigue microcracks that initiate fracture are located near elevated intracortical porosity but not elevated mineralization, J. Biomech. 47 (2014) 3135–3142, http://dx.doi.org/10.1016/j.jbiomech.2014.06.022.
[24] I. Masoud, F. Shapiro, R. Kent, A. Moses, A longitudinal study of the growth of the New Zealand white rabbit: cumulative and biweekly incremental growth rates for body length, body weight, femoral length, and tibial length, J. Orthop. Res. 4 (1986) 221–231, http://dx.doi.org/10.1002/jor.1100040211.

[25] A.A. Pampu, D. Dolanmaz, H.H. Tüz, M.C. Avunduk, R.S. Kissnissci, Histomorphometric evaluation of the effects of zoledronic acid on mandibular distraction osteogenesis in rabbits, J. Oral Maxillofac. Surg. 66 (2008) 905–910, http://dx.doi.org/10.1016/j.joms.2007.12.004.
[26] J.J. Kruzic, S.J. Kuskowski, R.O. Ritchie, Simple and accurate fracture toughness testing methods for pyrolytic carbon/graphite composites used in heart-valve prostheses, J. Biomed. Mater. Res. 74A (2005) 461–464, http://dx.doi.org/10.1002/jbm.a.30380.
[27] J.M. Deuerling, D.J. Rudy, G.L. Niebur, R.K. Roeder, Improved accuracy of cortical bone mineralization measured by polychromatic microcomputed tomography using a novel high mineral density composite calibration phantom, Med. Phys. 37 (2010) 5138–5145, http://dx.doi.org/10.1118/1.3480507.
[28] J.J. Broz, S.J. Simske, W.D. Corley, A.R. Greenberg, Effects of deproteinization and ashing on site-specific properties of cortical bone, J. Mater. Sci. Mater. Med. 8 (1997) 395–401, http://dx.doi.org/10.1023/A:1018545303184.
[29] Z. Manilay, E. Novitskaya, E. Sadovnikoy, J. McKittrick, A comparative study of young and mature bovine cortical bone, Acta Biomater. 9 (2013) 5280–5288, http://dx.doi.org/10.1016/j.actbio.2012.08.040.
[30] ASTM Standard E399-12, Standard Test Method for Linear-elastic Plane-strain Fracture Toughness K_{Ic} of Metallic Materials, American Society for Testing and Materials, West Conshohocken, PA, 2012http://dx.doi.org/10.1520/E0399.
[31] K.J. Koester, J.W. Ager, R.O. Ritchie, The true toughness of human cortical bone measured with realistically short cracks, Nat. Mater. 7 (2008) 672–677, http://dx.doi.org/10.1038/nmat2221.
[32] E.A. Zimmermann, R.O. Ritchie, Bone as a structural material, Adv. Healthc. Mater. 4 (2015) 1287–1304, http://dx.doi.org/10.1002/adhm.201500070.
[33] R.K. Nalla, J.J. Kruzic, R.O. Ritchie, Fracture in human cortical bone: local fracture criteria and toughening mechanisms, J. Biomech. 38 (2005) 1517–1525, http://dx.doi.org/10.1016/j.jbiomech.2004.07.010.
[34] R.K. Nalla, J.H. Kinney, R.O. Ritchie, Mechanistic fracture criteria for the failure of human cortical bone, Nat. Mater. 2 (2003) 164–168, http://dx.doi.org/10.1038/nmat832.
[35] M.S. Smith, Bone Fracture Toughness of Estrogen Deficient Rabbits(MS Thesis) West Virginia University, 2003.
[36] L.E. Bilston, D.G. Little, N.C. Smith, P. Williams, J. Briody, Zoledronic acid improves the mechanical properties of normal and healing bone, Clin. Biomech. 17 (2002) 716–718, http://dx.doi.org/10.1016/S0268-0033(02)00108-0.
[37] B.L. Pennypacker, L.T. Duong, T.E. Cusick, P.J. Masarachia, M.A. Gentile, J.-Y. Gauthier, W.C. Black, B.B. Scott, R. Samadfam, S.Y. Smith, D.B. Kimmel, Cathepsin K inhibitors prevent bone loss in estrogen-deficient rabbits, J. Bone Miner. Res. 26 (2011) 252–262, http://dx.doi.org/10.1002/jbmr.223.
[38] X. Wang, A.S. Shanbhag, H.E. Rubash, C.M. Agrawal, Short-term effects of bisphosphonates on the biomechanical properties of canine bone, J. Biomed. Mater. Res. 44 (1999) 456–460, http://dx.doi.org/10.1002/(SICI)1097-4636(19990315)44:4<456::AID-JBM12>3.0.CO;2-9.
[39] D.B. Burr, T. Diab, A. Koivunemi, M. Koivunemi, M.R. Allen, Effects of 1 to 3 years' treatment with alendronate on mechanical properties of the femoral shaft in a canine model: implications for subtrochanteric femoral fracture risk, J. Orthop. Res. 27 (2009) 1288–1292, http://dx.doi.org/10.1007/s00198-008-0754-4.
[40] C. Acevedo, H. Bale, B. Gludovatz, A. Wat, S.Y. Tang, M. Wang, B. Busse, E.A. Zimmermann, E. Schaible, M.R. Allen, D.B. Burr, R.O. Ritchie, Alendronate treatment alters bone tissues at multiple structural levels in healthy canine cortical bone, Bone 81 (2015) 352–363, http://dx.doi.org/10.1016/j.bone.2015.08.002.
[41] T. Mashiba, T. Hirano, C.H. Turner, M.R. Forwood, C.C. Johnston, D.B. Burr, Suppressed bone turnover by bisphosphonates increases microdamage accumulation and reduces some biomechanical properties in dog rib, J. Bone Miner. Res. 15 (2000) 613–620, http://dx.doi.org/10.1359/jbmr.2000.15.4.613.
[42] M.R. Allen, S. Reinwald, D.B. Burr, Alendronate reduces bone toughness of ribs without significantly increasing microdamage accumulation in dogs following 3 years of daily treatment, Calcif. Tissue Int. 82 (2008) 354–360, http://dx.doi.org/10.1007/s00223-008-9131-8.
[43] M.A. Gallant, D.M. Brown, J.M. Organ, M.R. Allen, D.B. Burr, Reference-point indentation correlates with bone toughness assessed using whole-bone traditional mechanical testing, Bone 53 (2013) 301–305, http://dx.doi.org/10.1016/j.bone.2012.12.015.
[44] D.B. Burr, Z. Liu, M.R. Allen, Duration-dependent effects of clinically relevant oral alendronate doses on cortical bone toughness in beagle dogs, Bone 71 (2015) 58–62, http://dx.doi.org/10.1016/j.bone.2014.10.010.
[45] W.G. Buettmann, M.J. Silva, Development of an *in vivo* bone fatigue damage model using axial compression of the rabbit forelimb, J. Biomech. 49 (2016) 3564–3569, http://dx.doi.org/10.1016/j.jbiomech.2016.08.020.
[46] N. Wasserman, B. Brydges, S. Searles, O. Akkus, *In vivo* linear microcracks of human femoral cortical bone remain parallel to osteons during aging, Bone 43 (2008) 856–861, http://dx.doi.org/10.1016/j.bone.2008.07.238.
[47] F. Erdogan, G.C. Sih, On the crack extension in plates under place loading and transverse shear, J. Basic Eng. 85 (1963) 519–527, http://dx.doi.org/10.1115/1.3656897.
[48] J.F. Throop, R.R. Fujczak, Stress, strain and deflection of cracked C-shaped specimens, Exp. Mech. 17 (1977) 290–296, http://dx.doi.org/10.1007/BF02324958.